Biometals (2012) 25:1023–1036
DOI 10.1007/s10534-012-9568-0

Characterization of the aqueous iron(III) chelation chemistry of a potential Trojan Horse antimicrobial agent: chelate structure, stability and pH dependent speciation

James M. Harrington · Tom Gootz · Mark Flanagan · Majinder Lall · John O'Donnell · Jennifer Winton · John Mueller · Alvin L. Crumbliss

Received: 19 January 2012 / Accepted: 5 July 2012 / Published online: 2 August 2012

Abstract The aqueous solution equilibria of a β-lactam antimicrobial agent containing a 3-hydroxy, 4-pyridinone group ($\mathbf{L}^{PF}$) binding to Fe(III) in aqueous solution has been characterized through spectrophotometric and potentiometric titrations. The metal-free ligand has four observable protonation constants, $pK_{a1} = 2.6$, $pK_{a2} = 3.43$, $pK_{a3} = 6.43$, and $pK_{a4} = 9.62$. $\mathbf{L}^{PF}$ forms a 3:1 ligand:Fe(III) complex in aqueous solution through coordinate-covalent bond formation exclusively involving the bidentate hydroxypyridinone moiety. This 3:1 $\mathbf{L}^{PF}$:Fe complex was found to have a stability constant of $\log \beta_{130} = 33.46$. A speciation diagram for the $\mathbf{L}^{PF}$ system demonstrates that in the region of physiological pH the tris-($\mathbf{L}^{PF}$)Fe(III) complex, $Fe(L^{PF})_3^{6-}$, predominates. This complex exhibits two irreversible reduction waves in solution at −30 mV versus NHE, corresponding to a ligand-based reduction, and at −385 mV versus NHE, corresponding to an irreversible Fe^{3+}/Fe^{2+} reduction of the $Fe(L^{PF})_3^{6-}$ complex.

Keywords Trojan horse · Antimicrobial · Chelation · Siderophore · Hydroxypyridinone · Iron · Redox

Introduction

Siderophores are microbially synthesized chelators that are specific for the solubilization and sequestration of iron(III), and subsequent cellular recognition and uptake (Crumbliss 1991; Crumbliss and Harrington 2009; Raymond and Dertz 2004; Stintzi and Raymond 2002). Bacterial requirements for iron and cell molecular recognition properties afforded by a ferri–siderophore complex, can be exploited in the design of highly effective therapeutic agents. Such Trojan Horse drugs are a class of molecules featuring antimicrobial agents that are delivered to the cell attached to recognition moieties that are taken up by the cell through normal avenues of transport (Miller et al. 2009). Iron is an essential nutrient and the Trojan Horse approach exploits the process of bacterial iron acquisition to produce a highly effective cell-targeted therapeutic agent. Trojan Horse drugs have the advantage that they may circumvent cell permeability and/or drug efflux problems associated with drug resistant bacterial strains. This Trojan Horse approach

Electronic supplementary material The online version of this article (doi:10.1007/s10534-012-9568-0) contains supplementary material, which is available to authorized users.

J. M. Harrington · A. L. Crumbliss (✉)
Department of Chemistry, Duke University, Durham, NC 27708-0346, USA
e-mail: alc@chem.duke.edu

T. Gootz · M. Flanagan · M. Lall · J. O'Donnell · J. Winton · J. Mueller
Pfizer Pharmatherapeutics, Groton Laboratories, 258 Eastern Point Rd., Groton, CT 06340-5146, USA

is used in nature by competing microbes, where the competitor microbe synthesizes a siderophore molecule linked to an antibiotic. This siderophore is called a sideromycin (Cheng et al. 2012). When the "enemy" micro-organism recognizes the iron-loaded sideromycin and brings it into the cell, the antibiotic tags along and ultimately brings cell death. Siderophore-drug conjugates hold the promise of microbe specific antibiotic therapies that may help retard antibiotic resistance. Consequently, the development of new Trojan Horse drugs is of considerable importance.

Infections by *Pseudomonas aeruginosa* and related bacteria contribute to a number of diseases in mammals and plants, and are of special concern in immune compromised patients (Rolston and Bodey 1992). Patients who suffer from severe burns or cystic fibrosis are particularly susceptible to diseases caused by *Pseudomonas*, which could result in complications in their treatment and possibly death. Due to the risk associated with *Pseudomonas* infection and the possibility of the development of multi-drug resistant strains of *Pseudomonas*, developing new and effective treatments for *Pseudomonas* infections is highly desirable. One attractive avenue for the development of therapeutic agents to address the rise of multi-drug resistant *Pseudomonas* infections is the use of Trojan Horse drugs.

There are presently a number of proposed and commercially available antimicrobial agents featuring the β-lactam moiety (Fig. 1), including penicillin, the cephalosporins, nocardicin A, aztreonam, and fortam. β-lactam antibiotics generally act by inhibiting proper formation of the peptidoglycan cell wall of the bacterium, which leads to death (Tipper 1985). Aztreonam (Fig. 1) has shown high efficacy against a range of Gram-negative bacteria, but it has been found to be ineffective at treating infections of *Pseudomonas* species of bacteria (Edwards et al. 1989; Sentochnik et al. 1989). Pirazmonam (Fig. 2) is a Trojan Horse molecule containing a β-lactam antibiotic that has been developed based on bacterial iron uptake systems (Sykes 1988). It features high structural similarity to aztreonam attached to a 3-hydroxy-4-pyridinone iron chelating group. Hydroxypyridinones form strong complexes with iron(III) and the iron bound moiety is recognized by Fiu and Cir outer membrane proteins in bacteria. (Crumbliss and Harrington 2009; Cheng et al. 2012).

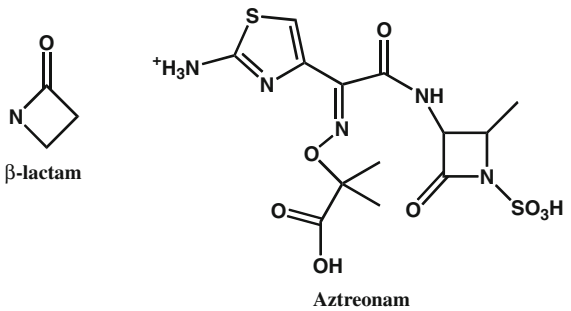

Fig. 1 Structure of the β-lactam moiety utilized in antimicrobial agents, such as the commercially-available Aztreonam

A more recently-developed Trojan Horse molecule featuring the 3-hydroxy-4-pyridinone moiety is U-78608. U-78608 ($\mathbf{L}^{PF}$, where the symbol $\mathbf{L}^{PF}$ represents the molecule U-78608 in all of its collective protonation states, which are individually referred to as: $H_4L^{PF\,1+}$, H_3L^{PF}, $H_2L^{PF\,1-}$, $HL^{PF\,2-}$, and $L^{PF\,3-}$, shown in Fig. 2), is a β-lactam-based molecule, which has interesting potential as an antimicrobial agent. U-78608 also contains a 3-hydroxy-4-pyridinone moiety, intended to facilitate chelation of iron and cellular recognition/uptake. This functionalization of the antimicrobial agent for iron binding can potentially promote uptake of the molecule by the microbe through normal siderophore-transport routes in some species of bacteria that have proven resistant to other β-lactam-based antimicrobial agents. The significant difference between the structure of pirazmonam and U-78608 (Fig. 2) is that the latter features one fewer amide functional group. This provides fewer sites where a peptidase can separate the β-lactam group from the iron-binding moiety, which makes U-78608 less susceptible to degradation in a biological system. U-78608, $\mathbf{L}^{PF}$, has been found to have a low minimal inhibitory concentration in *P. aeruginosa* compared to aztreonam and similar MIC values to aztreonam for other Gram-negative bacteria (Zurenko et al. 1990). It has also been shown that $\mathbf{L}^{PF}$ has much lower affinity for penicillin-binding protein than aztreonam in some species of Gram-negative bacteria (Zurenko et al. 1990). These findings suggest that $\mathbf{L}^{PF}$ is an effective antimicrobial agent for *Pseudomonas* infections, although the mechanism of action is unclear. Based on the structure of the molecule, it seems likely that the affinity of the molecule for binding iron is related to its antimicrobial properties. It has also been shown that in addition to being more effective than pirazmonam, $\mathbf{L}^{PF}$ exhibits a greater serum half-life than pirazmonam,

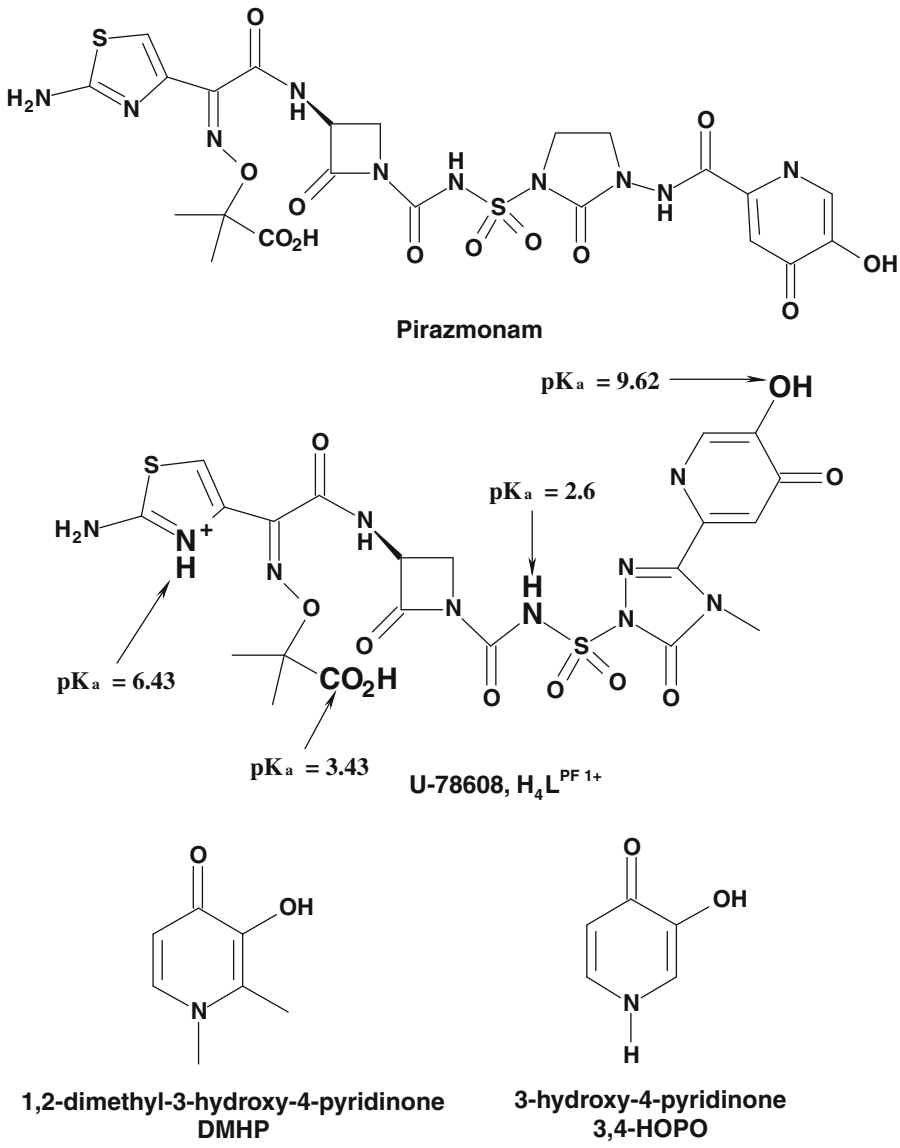

Fig. 2 Representative structures of β-lactam based Trojan Horse antibiotics, pirazmonam and U-78608 (L^{PF}). The ionizable groups of L^{PF} are highlighted in *bold*. Also shown are the analogous hydroxypyridinone iron chelators, 1,2-dimethyl-3-hydroxy-4-pyridinone, DMHP, and 3-hydroxy-4-pyridinone, 3,4-HOPO

making it a potential antimicrobial agent of interest for future development (Zurenko et al. 1990).

The purpose of this study is to examine the iron complexing capabilities of $\mathbf{L}^{PF}$ to determine the mode of iron binding, complex stoichiometry, complex stability, and redox characteristics. This has been done through a series of potentiometric and spectrophotometric titrations, as well as electrochemical characterization of the iron complex over a range of pH values. This characterization yields information on the potential role of iron binding in the effectiveness of $\mathbf{L}^{PF}$ as an antimicrobial agent.

Experimental

Materials

$NaClO_4$ (solid, Fisher) was obtained for preparation of background electrolyte. Solutions of NaOH and $HClO_4$ were prepared and standardized to the phenolphthalein endpoint against KHP and standardized NaOH, respectively. Stock solutions of $Fe(ClO_4)_3$ in 0.10 M $HClO_4$ were prepared and standardized by reduction with $SnCl_2$ and titration with $K_2Cr_2O_7$ (Vogel 1961).

Preparation of $\mathbf{L}^{PF}$

Samples of $\mathbf{L}^{PF}$ have been obtained from Pfizer, prepared as was previously reported and shown in Scheme S1 (see Supporting Information) (Barbachyn and Tuominen 1990). The crude product was dissolved in a minimum volume of DMSO, filtered and purified by preparative HPLC (Symmetry C8, 13–33 % acetonitrile in water with 0.1 % formic acid modifier). The pooled fractions were concentrated using the rotary evaporator to afford $\mathbf{L}^{PF}$ as a light pink solid. LCMS *m/z* 652.9 (M-1). ^{1}H NMR (400 MHz, DMSO-d_6) δ 9.01 (d, $J = 8.2$ Hz, 1H), 8.01 (s, 1H), 7.37 (s, 1H), 6.82 (s, 1H), 4.90 (m, 1H), 3.70 (m, 1H), 3.35–3.39 (br s, 4H), 1.42 (s, 6H).

Protonation constant determination

The protonation constants of $\mathbf{L}^{PF}$ were characterized by spectrophotometric titration of the molecule in the absence of iron(III). Spectrophotometric titrations were performed on solutions of 30 μM ligand in 0.10 M $NaClO_4$ background electrolyte. Solution pH was adjusted by titration with 0.10 M NaOH. All pH measurements were made with an Orion 230 A+ pH/ion meter equipped with an Orion Ross pH electrode filled with 3 M NaCl solution. The electrode was calibrated by the "classical method," titration of standardized 0.10 M $HClO_4$ with standardized 0.10 M NaOH (Martell and Motekaitis 1992). Calibration data were analyzed using the computer program, GLEE (Gans and O'Sullivan 2000). UV–Visible spectra were recorded with the Cary-50 spectrophotometer equipped with an external dip probe (Hellma, USA). Analysis of the measured spectra was performed using the program, HYPERQUAD, using a 4-proton model (Gans et al. 1996).

Solution equilibria

A spectrophotometric titration was performed to determine the stoichiometry of the Fe(III)–$\mathbf{L}^{PF}$ complex. The titration was performed by starting with a solution of a fixed ratio of Fe(III) to ligand and adding a solution of free ligand in a buffered solution at pH 7.0 in measured volumes. The initial solution was prepared at a molar ratio of 2 mol Fe(III) to 3 mol ligand. The ratio of moles ligand per mole Fe(III) was raised in a series of 2.0 mL aliquots and UV–Visible spectra were measured for the complexes over a range of Fe:$\mathbf{L}^{PF}$ molar ratios.

To characterize the stability constant of the fully formed complex, a spectrophotometric titration was performed to monitor the competition reaction between the Fe(III)–$\mathbf{L}^{PF}$ complex and EDTA, a common chelating agent traditionally used in competition experiments due to its high stability constant with Fe(III) and well-characterized spectral characteristics. A solution was prepared at a 1:5 molar ratio of Fe(III):$\mathbf{L}^{PF}$ at a pH of 6.03 in solution buffered with 0.25 M MES. Additions of 0.10 M EDTA solution in the MES buffered solution over a range of EDTA:-Fe(III) ratios from 0:1 to 10:1 were performed and spectra were measured at each EDTA concentration after allowing overnight equilibration. The equilibrium monitored in this reaction is shown in Eqs. 1–2. Spectra measured in the competition reaction with

$$\mathrm{Fe}\left(\mathrm{L}^{PF}\right)_3^{6-} + \mathrm{H_2EDTA}^{2-} + \mathrm{H}^{+} \rightleftarrows \mathrm{Fe(EDTA)}^{-} + 3\mathrm{H_2L}^{PF-} \quad (1)$$

$$K_{obs} = \frac{\left[\mathrm{Fe(EDTA)}^{-}\right]\left[\mathrm{H_2L}^{PF-}\right]^3}{\left[\mathrm{Fe}\left(\mathrm{L}^{PF}\right)_3^{6-}\right]\left[\mathrm{H_2EDTA}^{2-}\right]\left[\mathrm{H}^{+}\right]} \quad (2)$$

EDTA are shown in Fig. 3. The equilibrium spectra were analyzed with the program, HYPERQUAD, using a model featuring only one pK_a from $\mathbf{L}^{PF}$ corresponding to the hydroxypyridinone group, the determined iron-binding group of the molecule.

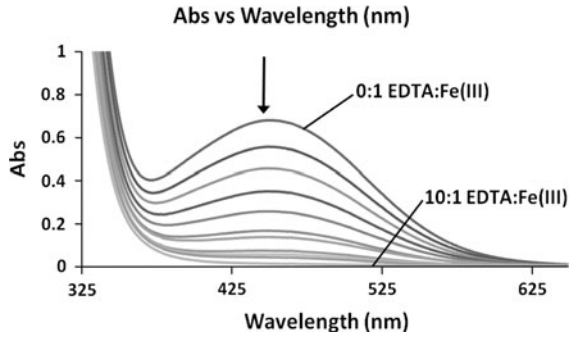

Fig. 3 UV–Visible spectra obtained from the competition experiment between $Fe(L^{PF})_3^{6-}$ and EDTA (Eq. 1). The concentration ratio of EDTA to iron(III) ranges from 0 equivalents EDTA to 10 equivalents EDTA. Experiment was performed in MES buffer at pH 6.03, T = 25 °C and $\mu = 0.10$ M ($NaClO_4$)

pH-dependent spectrophotometric titrations were performed to characterize the Fe(III):$\mathbf{L}^{PF}$ composition of the complexes over a range of pH values and to determine the stability constants of each complex. Three separate sets of titrations were performed, going from low pH to high pH (pH 2–11), high to low pH (pH 12–2) and low to lower pH (pH 6 to approximately 0.5). In all three titrations, 1:5 molar ratio of Fe(III):$\mathbf{L}^{PF}$ solutions were prepared in 0.10 M $NaClO_4$. In the low-to-high pH titration, the solution was titrated with standardized 0.10 M NaOH. In the high-to-low pH titration, the solution was titrated with 0.10 M $HClO_4$. In the low-to-lower pH titration, the solution was titrated with 1.0 M $HClO_4$. In the high-to-low titration and the low-to-lower pH titration, 15 min equilibration time was given after each addition to ensure complete reaction. Spectra were analyzed with the program HYPERQUAD to determine the stepwise equilibrium constants for the Fe–$\mathbf{L}^{PF}$ complexes (Gans et al. 1996).

HPLC/ESI/MS/MS characterization of Fe:L_3^{PF} complex

A 1 mL solution consisting of 50 μM $Fe(ClO_4)_3$ and 75 μM $\mathbf{L}^{PF}$ was prepared in 25 mM Tris–HCl pH 7.0. The reaction was allowed to proceed for 15 min at room temperature prior to transferring 200 μL to an HPLC injection vial. HPLC/ESI/MS/MS analysis was performed using a Shimadzu LC-20AD HPLC in line with a Sciex API-3000 triple quadrupole mass spectrometer operated in the positive ion mode. Post column flow was split such that mobile phase was introduced into the mass spectrometer at a rate of 100 μL/min. The ion spray interface temperature was 300 °C and the ion spray voltage was set at 3.5 kV. The orifice voltage was optimized at 40 eV and the sample injection volume was 10 μL. Nitrogen was used as both the nebulizing and collision gas. Total ion (Q1) experiments were performed at a range of 75–1,000 *m/z* at unit resolution. A collision energy of 20 eV was used for collision induced dissociation (CID) product ion scan experiments. Separation of the iron-ligand complex and free $\mathbf{L}^{PF}$ was achieved on a Phenomenex Onyx Monolithic C18 column (3 × 100 mm) utilizing a binary HPLC gradient consisting of 90:10 0.1 % formic acid : acetonitrile (mobile phase A) and acetonitrile (mobile phase B). The HPLC gradient schedule consisted of the following:

Time (min)	Flow rate	A (%)	B (%)
0	850	90	10
6	850	90	10
6.1	850	5	95
11.1	850	5	95
11.2	850	90	10
12.8	850	90	10

Electrochemical studies of the Fe-L^{PF} system

Cyclic voltammetric experiments were performed on the Fe(III)-$\mathbf{L}^{PF}$ system. A 1:5 Fe(III):$\mathbf{L}^{PF}$ solution was prepared in 0.10 M $NaClO_4$ and was titrated with 0.10 M NaOH. Measurements were taken using a BASi controlled growth mercury electrode set to the static Hg drop electrode mode as the working electrode, a Ag/AgCl (3.5 M KCl) reference electrode and a platinum wire auxiliary electrode. The working electrode potential was controlled by a Princeton Applied Research Model 263 potentiostat, controlled by the PowerSuite computer software. The solution pH was varied using standardized NaOH over the range of 1–9 and cyclic voltammograms were measured periodically. To investigate the possibility of reduction of the ligand, a cyclic voltammogram was measured for a solution of $\mathbf{L}^{PF}$ in the absence of iron in a solution buffered at pH 7.2. All potentials are reported versus NHE by applying a 205 mV correction to the observed values.

Results and discussion

Ligand protonation constants

Characteristic spectra obtained from the spectrophotometric pH titration of $\mathbf{L}^{PF}$ are shown in Fig. 4. Over the pH range of approximately pH 2–12, there are three separate equilibria observed, as suggested by three distinct pH ranges where isosbestic points were observed: the pH ranges of 2.1–5.6, 6.9–9.2, and above 10. It can be inferred from the structure of $\mathbf{L}^{PF}$ that the molecule contains four proton ionizable groups, shown in bold in Fig. 1. However, the three pH ranges where isosbestic points were observed suggest that only three ionizable protons are observed during the spectrophotometric titration. This suggests that the

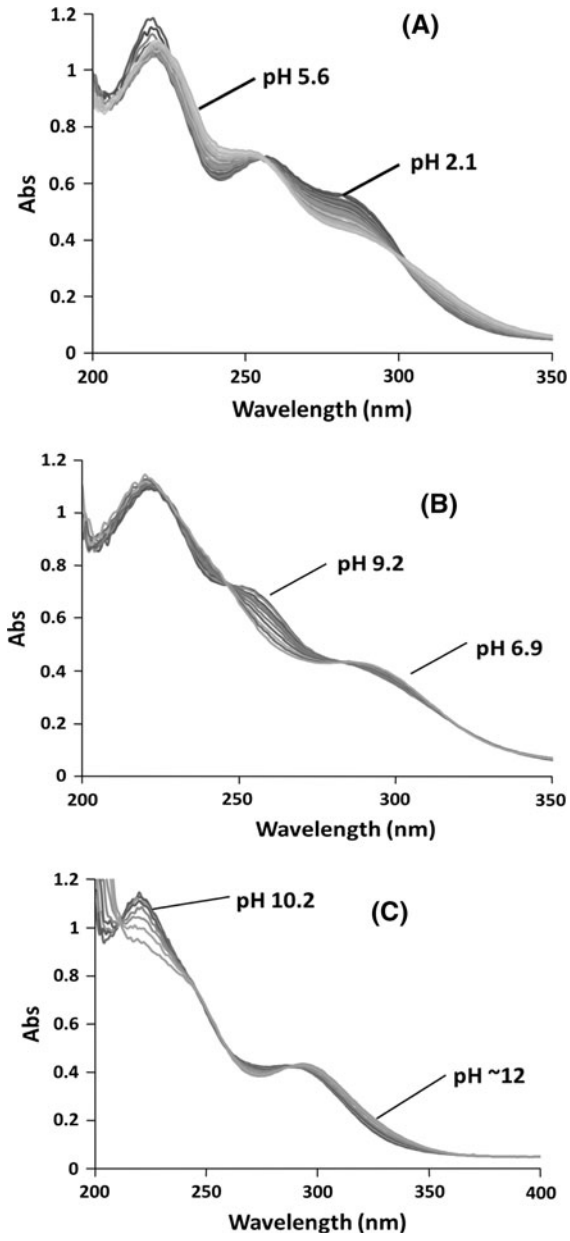

Fig. 4 Spectra of three separate equilibria observed in the spectrophotometric titration of L^{PF}. $[L^{PF}]_{tot} = 30$ μM, $\mu = 0.10$ M ($NaClO_4$), T = 25 °C. **A** pH 2.1–5.6, **B** pH 6.9–9.2, **C** above pH 10

fourth ionizable proton either was deprotonated in the initial spectrum that was measured and the protonation constant was too low to be observed during the course of the experiment, or that the final deprotonation reaction was spectrally silent. The optimal fit of the experimental data was obtained by using a 3-proton model, which provides evidence that the former explanation (low protonation constant) is more appropriate. An estimate of the value of the additional protonation constant is proposed by comparison to literature values of the structure of the fourth ionizable group. Protonation constants were determined from three replicate titrations using the program, HYPERQUAD using a 3-proton model, and the resulting pK_a's of all four ionizable groups are shown in Table 1 and Fig. 1.

The pK_a values measured are consistent with expected ranges of protonation constants of the predicted ionizable groups, hydroxypyridinone moieties ($pK_a \sim 9$), carboxylic acid moieties ($pK_a \sim 4$), and aminothiazole moieties ($pK_a \sim 6$) (Forlani et al. 2006; Scarrow et al. 1985). The structure of $\mathbf{L}^{PF}$ contains a fourth ionizable moiety, a sulfonamide proton (Fig. 2). A literature report of the protonation of a sulfonamide donor group suggests a pK_a close to 2.6, which would not be observable at the pH range over which the potentiometric titration experiment was performed and likely would have a minimal effect on the spectrum of the molecule in solution (Williamson et al. 1987). The value determined for the protonation constant of the 3,4-hydroxypyridinone group ($pK_a = 9.62$) is slightly higher than might be expected for a 3,4-HOPO group. This is likely due to one possible resonance form of the hydroxypyridinone donor group, which results in additional electron density being concentrated on the carbonyl oxygen donor atom of the 3,4-HOPO group, shown in Eq. 3 below. This electron density shift through resonance would enhance the formation of a hydrogen bond between the hydroxyl proton and the carbonyl oxygen, thus decreasing its acidity. A speciation diagram for the protonation of $\mathbf{L}^{PF}$ is shown in Fig. 5A.

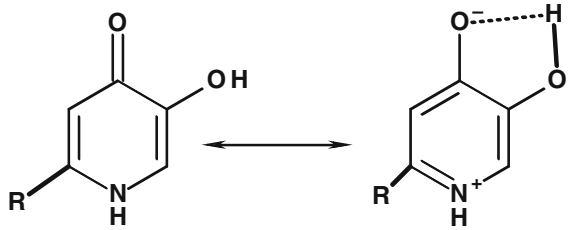

3

Iron complex equilibria: complex structure

It was observed that in the preparation of these solutions, at low ligand/iron molar ratios such as 1:1,

Table 1 Equilibrium constants determined for the proton-dependent and proton-independent reactions of $\mathbf{L}^{PF}$ with Fe(III)

Reaction	K or β	log K or log β
$L^{PF\,3-} + H^+ \rightleftarrows HL^{PF\,2-}$	pK_{a4}	9.62 (0.07)
$HL^{PF\,2-} + H^+ \rightleftarrows H_2L^{PF\,-}$	pK_{a3}	6.43 (0.03)
$H_2L^{PF\,-} + H^+ \rightleftarrows H_3L^{PF}$	pK_{a2}	3.43 (0.09)
$H_3L^{PF} + H^+ + \rightleftarrows H_4L^{PF+}$	pK_{a1}	2.6 (0.2)
$Fe(H_2O)_6^{3+} + 3L^{PF\,3-} \rightleftarrows Fe(L^{PF})_3^{6-} + 6H_2O$	β_{130}	33.46 (0.02)[a]
$Fe(H_2O)_6^{3+} + 3HL^{PF\,2-} \rightleftarrows Fe(L^{PF})_3^{6-} + 3H^+ + 6H_2O$	K_{130}	4.6 (0.1)[a]
$Fe(H_2O)_6^{3+} + 2L^{PF\,3-} \rightleftarrows Fe(L^{PF})_2(H_2O)_2^{3-} + 4H_2O$	β_{120}	22.66 (0.09)[a]
$Fe(L^{PF})_2(H_2O)_2^{3-} + L^{PF\,3-} \rightleftarrows Fe(L^{PF})_3^{6-}$	β_3	10.80 (0.09)[a]
$Fe(L^{PF})_2(H_2O)_2^{3-} + HL^{PF\,2-} \rightleftarrows Fe(L^{PF})_3^{6-} + H^+$	K_3	1.1 (0.1)[a]
$Fe(H_2O)_6^{3+} + 2HL^{PF\,2-} \rightleftarrows Fe(L^{PF})_2(H_2O)_2^{3-} + 2H^+ + 4H_2O$	K_{120}	3.4 (0.1)[a]
$Fe(H_2O)_6^{3+} + L^{PF\,3-} \rightleftarrows Fe(L^{PF})(H_2O)_4 + 2H_2O$	β_{110}	11.36 (0.04)[a]
$Fe(H_2O)_6^{3+} + HL^{PF\,2-} \rightleftarrows Fe(L^{PF})(H_2O)_4 + H^+ + 2H_2O$	K_{110}	1.74 (0.08)[a]
$Fe(L^{PF})(H_2O)_4 + L^{PF\,3-} \rightleftarrows Fe(L^{PF})_2(H_2O)_2^{3-} + 2H_2O$	β_2	11.30 (0.09)[a]
$Fe(L^{PF})(H_2O)_4 + HL^{PF\,2-} \rightleftarrows Fe(L^{PF})_2(H_2O)_2^{3-} + H^+ + 2H_2O$	K_2	1.7 (0.1)[a]
$Fe(L^{PF})_3^{6-} \rightleftarrows Fe(L^{PF})_3H_{-1}^{7-} + H^+$	K_{aFe1}	9.0 (0.2)[b]
$Fe(L^{PF})_3H_{-1}^{7-} \rightleftarrows Fe(L^{PF})_3H_{-2}^{8-} + H^+$	K_{aFe2}	9.9 (0.4)[b]

[a] For simplicity, the level of protonation of $\mathbf{L}^{PF}$ in equilibrium reactions with Fe^{3+} only reflects the HOPO chelating moiety. See text for further discussion

[b] The equilibria shown in these equations represent the sequential loss of two protons from the $Fe(L^{PF})_3^{6-}$ complex at higher pH

Numbers shown in parentheses are the standard deviation of the value as determined from the program, HYPERQUAD (Gans et al. 1996). All experiments were performed at T = 25 °C and μ = 0.10 M ($NaClO_4$)

iron(III) precipitates in the form of a brown solid, presumably iron hydroxide, in the pH range of approximately 2–3, followed by a slow dissolution at higher pH values (dissolution time varying from 5 min to 2 h dependent on the concentration of the ligand and the solution pH). A minimum molar ratio of 2 Fe:3 $\mathbf{L}^{PF}$ prevents precipitation of iron(III), and a decrease in the Fe:$\mathbf{L}^{PF}$ ratio resulted in increased complex formation through 1:4 Fe:$\mathbf{L}^{PF}$ ratio (Fig. S1, Supporting Information). A graph of the absorbance measured at λ_{max} = 449 nm from these solutions, adjusted for dilution, plotted as a function of the number of moles of ligand per mole Fe(III) is shown in Fig. S2. These data suggest that the equilibria occurring in solution at our experimental conditions involves the formation of a Fe($\mathbf{L}^{PF}$)$_3$ complex. The results of the titration were also used to calculate the λ_{max} and molar absorptivity of the Fe($\mathbf{L}^{PF}$)$_3$ complex (Table 2).

The spectra measured from pH-dependent spectrophotometric titrations of the system are shown in Figs. S3–S4, where clean isosbestic points indicated conversion between two iron complexes. In the low-to-high pH titration (Fig. S3), one spectral shift was observed over the pH range of 2.3–5.5, with an initial λ_{max} of 483 nm and a final λ_{max} of 452 nm. A second equilibrium was observed over the range of pH 6.1–7.9, with a final λ_{max} of 458 nm. The final shift was observed from pH 8.2 to 10.6, with a λ_{max} of 472 nm. A second spectrophotometric titration from pH 6 to ~0.4 (Fig. S4) exhibited a second spectral transition below pH 2.7 (Fig. S4B), where the λ_{max} increased from 481 nm and the spectral intensity decreased, partly due to dilution from increasing volumes required to change the pH. The shifts in spectral handles over a range of solution pH values can be used to characterize the species present in solution, as well as the $\mathbf{L}^{PF}$ complex equilibria (shown in Table 1), as will be discussed later.

The composition of the species observed in these equilibria was determined by comparison of the λ_{max}

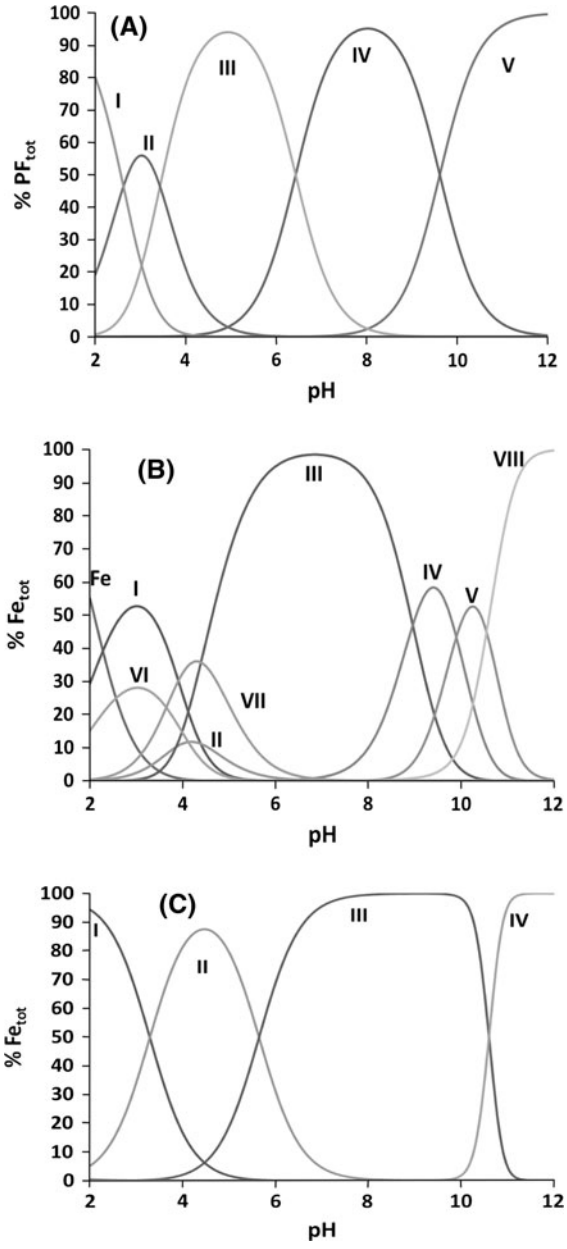

◀ **Fig. 5** Speciation diagram for **A** the free ligand L^{PF}, **B** the Fe(III)-L^{PF} system and **C** the Fe(III)-DMHP system, calculated using equilibrium constants reported here and in the literature (Ramunas et al. 1991). The plots show relative amounts of total iron in different forms over a range of pH values. Panel **A**, $[Fe^{3+}]_{tot} = 0$ M, $[\mathbf{L}^{PF}]_{tot} = 10^{-5}$ M, T = 25 °C and $\mu = 0.10$ ($NaClO_4$). Panels **B** and **C**, $[Fe^{3+}]_{tot} = 10^{-6}$ M, $[L]_{tot} = 10^{-5}$ M, T = 25 °C and $\mu = 0.10$ ($NaClO_4$). Key: (A) I = $H_4L^{PF\,+}$, II = H_3L^{PF}, III = H_2L^{PF-}, IV = $HL^{PF\,2-}$, and V = $L^{PF\,3-}$. (B) I = $Fe(L^{PF})(H_2O)_4$, II = $Fe(L^{PF})_2(H_2O)_2^{3-}$, III = $Fe(L^{PF})_3^{6-}$, IV = $Fe(L^{PF})_3H_{-1}^{7-}$, and V = $Fe(L^{PF})_3H_{-2}^{8-}$. VI–VIII represent hydrolyzed forms of free metal ion, $Fe(OH)^{2+}$, $Fe(OH)_2^{+}$, and $Fe(OH)_4^{-}$, respectively. See text and footnotes (a) and (b) in Table 1. **C** I = $Fe(DMHP)(H_2O)_4^{2+}$, II = $Fe(DMHP)_2(H_2O)_2^{+}$, III = $Fe(DMHP)_3$, and IV = $Fe(OH)_4^{-}$. In both **B** and **C**, Fe represents free aqueous iron(III), $Fe(OH_2)_6^{3+}$

values observed in the spectrophotometric titrations with the observed λ_{max} values of 3-hydroxy-4-pyridinone complexes from a previous study (Table 2) (Scarrow et al. 1985). This suggests that the binding mode of the ligand to iron(III) is exclusively through the 3-hydroxy-4-pyridinone donor group (Fig. 6). The observed λ_{max} of the solution around pH 2.5 and 6.1 correspond closely to the literature values (Table 2), suggesting binding of $\mathbf{L}^{PF}$ with Fe(III) through the hydroxypyridinone moiety, with additional loss of protons from the complex above pH 6.1 at remote sites on the ligand.

Additional evidence for the proposed complex structure (Fig. 6) was provided by HPLC/ESI-MS/MS characterization of the complex in solution. $\mathbf{L}^{PF}$ and the proposed iron-ligand complex exhibited retention times of 1.75 and 0.98 min respectively (Fig. S5). In the positive ion mode, $\mathbf{L}^{PF}$ exhibited a peak at 655 *m/z* units ($C_{21}H_{23}N_{10}O_{11}S_2^{+}$, Fig. S6A) and the iron complex showed a peak at 673 *m/z* units, which is consistent with a 1:3 Fe:$\mathbf{L}^{PF}$ ratio ($C_{63}H_{66}FeN_{30}O_{33}S_6^{3+}/3+ = 673$ *m/z*, Fig. S7A). Further LC/MS/MS structural confirmation was made using CID product ion scans at 655 *m/z* units (Fig. S6B) and 673 *m/z* units (Fig. S7B) for $\mathbf{L}^{PF}$ and the iron–ligand complex, respectively. Both product ion spectra

Table 2 Observed wavelengths of maximum absorbance for the iron(III)-$\mathbf{L}^{PF}$ complex system and molar absorptivities of the complexes, calculated by the program HYPERQUAD (Gans et al. 1996)

Complex	λ_{max} (nm) L = $\mathbf{L}^{PF}$	ε (M^{-1} cm^{-1}) L = $\mathbf{L}^{PF}$	$\lambda_{max,}$ (nm)[a] L = DMHP
FeL	543	2660	538
FeL_2	499	4480	488
FeL_3	451	7160	446
FeL_3H_{-}	458	5895	
FeL_3H_{2-}	472	6950	

Literature values for the FeL through FeL_3 complexes of the iron(III)-DMHP system are shown for comparison. L represents the respective hydroxypyridinone-donor chelators, $\mathbf{L}^{PF}$ or DMHP

[a] Literature values are taken from (Ramunas et al. 1991)

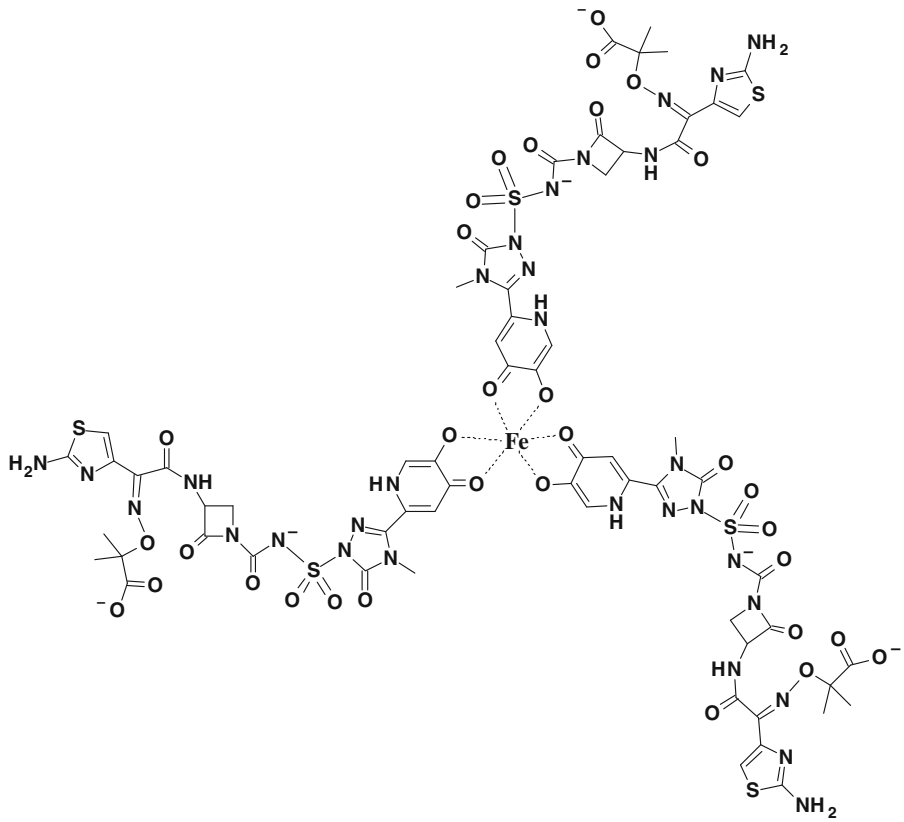

Fig. 6 Proposed structure of the 1:3 Fe–L^{PF} complex at physiological pH, $Fe(L^{PF})_3^{6-}$

revealed major ions at *m/z* 126 and *m/z* 209 consistent with fragmentation at the 5-imino-2-aminothiazole and triazol-2-one-3-methyl-4-dihydroxypyridin-3-hydroxy-4-one moieties of $\mathbf{L}^{PF}$, respectively (Fig. S8). While these HPLC/ESI-MS/MS data confirm iron complexation through the hydroxypyridinone moiety to form $Fe(\mathbf{L}^{PF})_3$ in fully coordinated form, conditions of the experiments and the use of mixed organic solvents do not permit comparison with the pH dependent speciation studies described below and in Fig. 5B.

Iron complex equilibria: determination of stepwise formation constants

Due to the high affinity of the hydroxypyridinone moiety for iron(III), a spectrophotometric competition titration with EDTA was performed to indirectly determine the stability constant for the Fe(III)-$\mathbf{L}^{PF}$ system. While the stoichiometry of the fully formed Fe(III)–$\mathbf{L}^{PF}$ complex was determined to be 3:1, the ligand-to-metal molar ratio of 3:1 is insufficient to provide full formation of the $Fe(L^{PF})_3^{6-}$ complex (see Fig. S2). The EDTA competition experiment was designed at a 5:1 molar ratio of $\mathbf{L}^{PF}$:Fe, which gives complete formation of the $Fe(L^{PF})_3^{6-}$ complex. In computing the equilibrium constants of the Fe(III)-$\mathbf{L}^{PF}$ system, it is only necessary to use the protonation constant assigned to the hydroxypyridinone O–H proton, as this group is the only moiety involved in the binding interaction with iron(III), as deduced from the structure of the molecule, the stoichiometry of the complex at circumneutral pH and the spectral observations described in the previous section. Any further deprotonation reaction will affect the electrostatics of the interaction of the molecule with Fe^{3+}, but should not directly factor into the binding equilibria. The equilibrium constant for the formation of the $Fe(L^{PF})_3^{6-}$ complex is shown below and in Table 1. The value obtained from the EDTA competition titration is the proton independent stability constant, log β_{130} (Eqs. 4–5). However, in solution, protons will be

$$Fe^{3+} + 3L^{PF\,3-} \rightleftarrows Fe\left(L^{PF}\right)_3^{6-} \quad (4)$$

$$\beta_{130} = \frac{\left[\mathrm{Fe}\left(\mathrm{L}^{\mathrm{PF}}\right)_3^{6-}\right]}{\left[\mathrm{Fe}^{3+}\right]\left[\mathrm{L}^{\mathrm{PF}3-}\right]^3} = 10^{33.46} \quad (5)$$

present to compete with iron for binding to the hydroxypyridinone moiety (Eq. 6). Consequently it is necessary to determine the proton-dependent stability constants, which can be done by including the

$$\mathrm{Fe}^{3+} + 3\mathrm{HL}^{\mathrm{PF}2-} \rightleftarrows \mathrm{Fe}\left(\mathrm{L}^{\mathrm{PF}}\right)_3^{6-} + 3\mathrm{H}^{+} \quad (6)$$

protonation constant of the hydroxypyridinone moiety of the molecule in the data analysis. The proton-dependent and independent equilibria and determined stability constants for all complexes formed in the iron(III)-$\mathbf{L}^{\mathrm{PF}}$ system are shown in Table 1.

The value determined for the log β_{130} of the complex (Eqs. 4–5, log $\beta_{130} = 33.46$) is lower than that of unsubstituted 3,4-HOPO (log $\beta_{130} = 34.91$) or of 1,2-dimethyl-3-hydroxy-4-pyridinone (log $\beta_{130} = 35.88$) (Clarke and Martell 1992; Ramunas et al. 1991). This is likely due to differing acidity of the hydroxypyridinone donors and decreased electron donating ability of the $\mathbf{L}^{\mathrm{PF}}$ molecule due to the extensive conjugated electron system. Steric factors due to the bulky $\mathbf{L}^{\mathrm{PF}}$ backbone may also be a factor. The low-to-high pH titration of the $\mathrm{Fe}(\mathrm{L}^{\mathrm{PF}})_3^{6-}$ complex (Fig. S3) was used to determine the stability constant of the $\mathrm{Fe}(\mathrm{L}^{\mathrm{PF}})_2\,(\mathrm{OH}_2)_2\,^{3-}$ complex corresponding to Eq. 7. The spectra obtained from the spectrophotometric titration over the pH range of 2.1–6.5 were used

$$\mathrm{Fe}_{\mathrm{aq}}^{3+} + 2\mathrm{HL}^{\mathrm{PF}2-} \rightleftarrows \mathrm{Fe}\left(\mathrm{L}^{\mathrm{PF}}\right)_2(\mathrm{OH}_2)_2^{3-} + 2\mathrm{H}^{+} \quad (7)$$

with the program HYPERQUAD to determine the proton-independent equilibrium constant for the $\mathrm{Fe}(\mathrm{L}^{\mathrm{PF}})_2\,(\mathrm{OH}_2)_2\,^{3-}$ complex (Gans et al. 1996). The equilibrium constants involving the $\mathrm{Fe}(\mathrm{L}^{\mathrm{PF}})(\mathrm{OH}_2)_4$ complex were determined using spectra obtained from the spectrophotometric titration below pH 2.5 (Fig. S4B). Therefore, the values may be less accurate than the other determinations due to the high dilution factor.

The determined equilibrium constants and protonation constants were used to calculate the free iron concentration in solution, or pFe value, as a function of pH, shown in Fig. 7, and to calculate speciation models over a range of biologically relevant pH values (Fig. 5B). The pFe value is a measure of the unbound iron present in the system, not including hydrolyzed

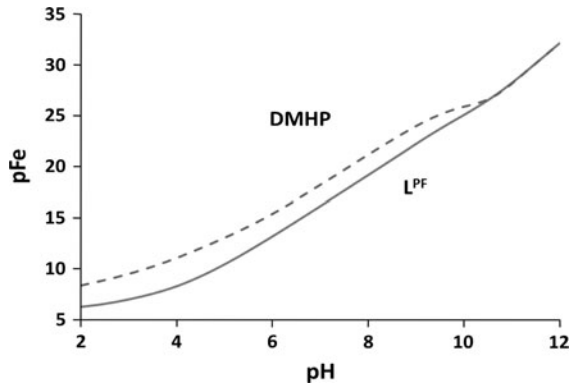

Fig. 7 Plot of pFe values over a range of pH values for the Fe(III)-L^{PF} system (*solid line*) and the Fe(III)-DMHP system (*dashed line*). For both graphs, $[\mathrm{Fe}^{3+}]_{\mathrm{tot}} = 10^{-6}$ M, $[\mathrm{L}]_{\mathrm{tot}} = 10^{-5}$ M, and all constants used in the analysis were measured at 25 °C and $\mu = 0.10$ ($\mathrm{NaClO_4}$)

forms of iron. The pFe value (Eq. 8) is normally calculated at some standard set of conditions,

$$\mathrm{pFe} = -\log\left[\mathrm{Fe}^{3+}\right]_{\mathrm{free}} \quad (8)$$

$[\mathrm{Fe}^{3+}]_{\mathrm{tot}} = 10^{-6}$ M, $[\mathbf{L}^{\mathrm{PF}}]_{\mathrm{tot}} = 10^{-5}$ M and pH 7.4, but it can also be useful to calculate pFe over a range of pH values, as the degree of complexation varies with pH (Harris et al. 1979). The calculated pFe value for the standard conditions at pH 7.4 is 17.3, relatively low for an iron chelator, and a plot of pFe values over a range of pH values is shown in Fig. 7. The determined pFe value is lower than that of 3,4-HOPO, the bidentate analog of $\mathbf{L}^{\mathrm{PF}}$ (Fig. 1, pFe = 20.72), as well as that of 1,2-dimethyl-3-hydroxy-4-pyridinone (DMHP, Fig. 1; pFe = 19.4). This is illustrated in Fig. 7. The differences in pFe values are due in part to the lower log β_{130} of the $\mathbf{L}^{\mathrm{PF}}$ complex compared to 3,4-HOPO and DMHP.

A speciation diagram for the Fe-$\mathbf{L}^{\mathrm{PF}}$ system over a range of pH values was generated using the determined stability constants (Table 1) to show the form of the complex at a variety of conditions (Fig. 5B). The speciation diagram of the Fe-$\mathbf{L}^{\mathrm{PF}}$ system is somewhat simplified from the actual speciation of the complex in solution. Below pH 5, the protonation constants of the carboxylate, aminothiazole and sulfonamide groups begin to factor into speciation of the ligand. As these groups are not involved in iron(III) complex formation, it is likely that the protonation constants of the groups will be minimally affected by the formation of the $\mathrm{Fe}(\mathrm{L}^{\mathrm{PF}})_{\mathrm{x}}^{\mathrm{n}-}$ complexes. This

suggests that at low pH values, the speciation of the $Fe(L^{PF})_x^{n-}$ complex will involve the additional protonation of the carboxylate, aminothiazole and sulfonamide moieties. The protonation states of those remote sites is important in considering the bioavailability of iron(III)–$\mathbf{L}^{PF}$ complexes, as the protonation of the remote sites will change the overall charge of the complex. Because of the deprotonation of the remote sites on the molecules, the overall charge of the $Fe(\mathbf{L}^{PF})_3$ complex at most biologically relevant conditions, pH 6.5–8, is 6−, while the $Fe(\mathbf{L}^{PF})_3$ complex exhibits an overall charge of 3− at pH values below 6.5.

The complex is seen to be relatively weak binding compared to other iron chelators, as at lower pH values, the ligand is not able to effectively compete with hydrolysis of the metal ion, as noted above. However, between pH 6 and 8.5, the concentration of unbound iron is low, indicating high stability of the complex around physiological pH. The speciation diagram of the Fe(III)-DMHP system is also shown for comparison (Fig. 5C). As suggested by the differences in stability constants, chelation by DMHP is more stable than that of $\mathbf{L}^{PF}$, resulting in the absence of hydrolyzed forms of the metal ion from the speciation diagram at low pH values. This observation is consistent with the formation of a hydroxide precipitate at lower pH values in the $\mathbf{L}^{PF}$ system. However, comparison of the two speciation diagrams shows that around physiological pH values, a higher percentage of iron is found as the FeL_3 complex in the presence of $\mathbf{L}^{PF}$ than in the presence of DMHP. This suggests that while the chelation of Fe(III) by $\mathbf{L}^{PF}$ is not stronger than DMHP (lower pFe values), $\mathbf{L}^{PF}$ is more likely to form the fully chelated complex at circumneutral pH than DMHP.

Electrochemical characterization of the Fe(III)-L^{PF} system

In vivo, the natural byproducts of some biological processes are peroxide and superoxide species, which can react with iron(III) via the Fenton cycle to form oxygen radicals and other reactive oxygen species that can damage the cell (Fenton 1894; Pierre and Fontecave 1999; Pierre et al. 2002). Chelation of iron(III) by some ligands shifts the redox potential of the Fe^{3+}/Fe^{2+} couple to more negative values, out of the range which will allow participation in Fenton chemistry (Crumbliss and Harrington 2009; Harrington and Crumbliss 2009). If a chelator is to be used as a therapeutic agent, it is important to ensure that the metal complex exhibits a reduction potential outside of the range of biological reductants to prevent redox cycling in the patient. Due to these factors, it was desirable to investigate the redox chemistry of the Fe(III)-L^{PF} system.

The cyclic voltammograms obtained for the Fe(III)-$\mathbf{L}^{PF}$ system can be placed into three groups according to pH ranges: pH $\sim$1 to $\sim$2.5; pH 2.5–4; and above pH 4. Representative voltammograms for these three regions are shown in Fig. 8. Below pH 2.5 (Fig. 8A), there were two observable irreversible reductions: a pH independent reduction peak current at ~ -500 mV versus NHE and a pH-dependent irreversible reduction peak current that moves over the range from 0 to −200 mV versus NHE. From pH 2.5 to 4 (Fig. 8B), the more negative reduction signal shifted to more negative potentials and decreased in intensity until it was replaced with a reduction peak current at −300 mV versus NHE. The more positive reduction peak current decreased in intensity until it was replaced with a reduction at −50 mV versus NHE. Above pH 4, there were two irreversible reductions observed, one pH-independent reduction peak current at −30 mV versus NHE and a second pH-dependent reduction peak current over the potential range of −300 to −415 mV versus NHE. At physiological pH, there are two irreversible reductions observed, with peak potentials at −30 mV versus NHE and −385 mV versus NHE (Fig. 8C).

The representative voltammograms in Fig. 8 correlate well with the pH dependent speciation diagram in Fig. 5B, as below pH 4, the predominant species is $Fe(L^{PF})(H_2O)_4$, with a large fraction of the iron found as the aquated or hydrolyzed ion. Above pH 4, the tris-coordinated complex, $Fe(L^{PF})_3^{6-}$ is predominant, and stable until about pH 9.

The cyclic voltammogram measured for $\mathbf{L}^{PF}$ in the absence of iron(III) is shown in Fig. S9. A single irreversible reduction is observed at −50 mV versus NHE, consistent with the observed higher (less negative) peak currents measured for the iron complex. This reduction can be assigned to the ligand β-lactam moiety. There have been studies performed on the electrochemical reduction of a variety of β-lactam-based antibiotics, including the structurally similar aztreonam, which shows an

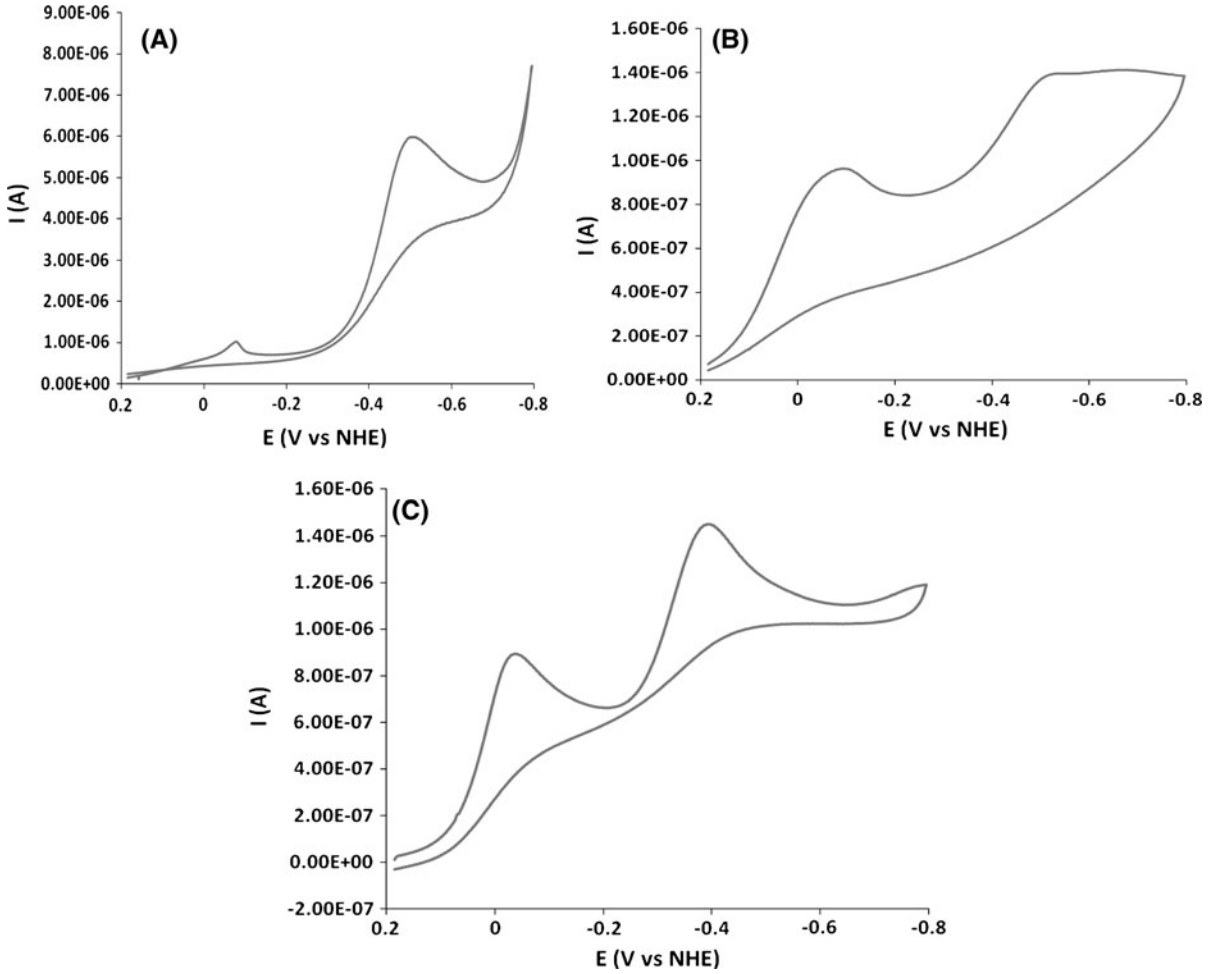

Fig. 8 Cyclic voltammetric titration of a 1:5 M:L molar ratio solution of the Fe(III)-$\mathbf{L}^{PF}$ system. Representative voltammograms are shown for the three pH ranges observed during the titration. **A** pH 1.4, $E_{red1} = -70$ mV versus NHE, $E_{red2} = -500$ mV versus NHE, **B** pH 3.8, $E_{red1} = -84$ mV versus NHE, $E_{red2} = -506$ mV versus NHE, **C** pH 7.4, $E_{red1} = -30$ mV versus NHE, $E_{red2} = -385$ mV versus NHE. Conditions: $[Fe^{3+}]_{tot} = 1$ mM, $[\mathbf{L}^{PF}]_{tot} = 5$ mM, T = 25 °C, $\mu = 0.20$ ($NaClO_4$), Reference electrode: Ag/AgCl, 3.5 M KCl, auxiliary electrode: platinum wire, working electrode: hanging drop mercury electrode, scan rate: 20 mV/sec

irreversible reduction occurring at a more negative potential around physiological pH ($E_{1/2} < -0.26$ V vs. NHE). This signal was proposed to correspond to the 2-proton reduction of the carbonyl moiety of the β-lactam group to a cyclobutanol moiety (El-Maali 1998). It is possible that the differing side chains connected to the β-lactam shift the reduction potentials to more positive values. The reduction potential of the irreversible reduction observed in the solution of $\mathbf{L}^{PF}$ alone occurs at the same potential as the corresponding irreversible reduction peak in the presence of iron. It seems unlikely that the presence of iron would shift the β-lactam reduction potential from those reported in the literature for similar structures.

In order to identify the Fe(III)-L^{PF} system signal produced by the Fe^{3+}/Fe^{2+} couple, cyclic voltammograms were obtained for Fe(III) in the presence of excess DMHP, as this ligand is an iron(III) binding site analogue for $\mathbf{L}^{PF}$. A representative cyclic voltammogram for Fe(III) in the presence of 5-fold excess DMHP is shown in Fig. S10. This shows a single reversible reduction with $E_{1/2}$ at -486 mV versus NHE at physiological pH. This is consistent with assigning the more negative peak in the Fe(III)-$\mathbf{L}^{PF}$ system to a Fe^{3+}/Fe^{2+} centered irreversible reduction.

The cyclic voltammogram of $Fe(DMHP)_3$ is quasi-reversible in nature, compared to the irreversibility of the Fe-$\mathbf{L}^{PF}$ system. Presumably the irreversible character comes from dissociation of Fe^{2+} from the Fe–$\mathbf{L}^{PF}$ complex upon reduction. The increased stability of the $Fe(DMHP)_3$ complex and the large excess of DMHP over Fe^{3+} prevents the complex dissociation event from occurring prior to re-oxidation. Additionally, this suggests that the dissociation kinetics of reduced ferrous form, $Fe(L^{PF})_3^{7-}$, is rapid. This is illustrated in Eq. 9.

$$Fe^{3+}\left(L^{PF}\right)_3^{6-} + \varepsilon^- \rightarrow Fe^{2+}\left(L^{PF}\right)_3^{7-} \rightarrow Fe_{aq}^{2+} + 3L^{PF\,3-} \quad (9)$$

This Fe^{3+}/Fe^{2+} centered reduction for $Fe(L^{PF})_3^{6-}$ occurs at a more positive potential (−385 mV) than other siderophore and siderophore mimic systems, and is more positive than other iron-bidentate hydroxypyridinone complexes, possibly due to the presence of the extended conjugated electron system of the backbone. However, the redox potential assigned to the Fe^{3+}/Fe^{2+} couple in $Fe(L^{PF})_3^{6-}$ is too negative to participate in the Haber–Weiss cycle to produce toxic ROS (Harrington and Crumbliss 2009).

Conclusions

The molecule $\mathbf{L}^{PF}$ has been shown to be a relatively strong chelator of iron(III) at physiological pH, although the strength of binding is less than analogous hydroxypyridinone chelators. Iron(III) binding occurs through the 3-hydroxy-4-pyridinone donor group and allows the formation of a 3:1 L:Fe complex (Fig. 6). pH dependent protonation equilibria were observed and the overall complex $Fe^{3+}(L^{PF})_3^{6-}$ carries a 6− charge at physiological pH 7–8. The formation of an iron(III) complex may provide the mechanism for Trojan Horse antimicrobial activity. The redox chemistry of the complex is pH dependent and the complex exhibits two irreversible reductions, one corresponding to bound iron(III) and another corresponding to the $\mathbf{L}^{PF}$ ligand. The observed redox behavior of the iron(III) complex suggests that it will not participate in deleterious redox reactions leading to ROS at physiological conditions. The weaker iron(III) affinity of $\mathbf{L}^{PF}$ relative to some natural siderophores makes it unclear whether it is able to compete with natural metal chelators for iron(III); however, the effectiveness of $\mathbf{L}^{PF}$ as an antimicrobial agent makes it a vehicle for additional drug development.

Acknowledgments ALC thanks the NSF (Grant CHE0809466) for funding and the Duke Center for Biomolecular and Tissue Engineering for partial financial support for JMH.

References

Barbachyn MR, Tuominen TC (1990) Synthesis and structure-activity relationships of monocarbams leading to U-78608. J Antibiot 43:1199–1203

Cheng J, Juarez-Hernandez RE, Miller MJ (2012) Exploring bacterial iron acquisition: siderophore conjugates. Future Med Chem 4:297–313

Clarke ET, Martell AE (1992) 1-Methyl-3-hydroxy-2-pyridinone and 1,4-dihydroxy-2-pyridinone complexes of the trivalent metal ions of Fe(III), Ga(III), Al(III), In(III) and Gd(III): potentiometric and spectrophotometric determination of stabilities. Inorg Chim Acta 196:185–194

Crumbliss AL (1991) Aqueous solution equilibrium and kinetic studies of iron siderophore and model siderophore complexes. In: Winkelmann G (ed) Handbook of microbial iron chelates. CRC Press, Boca Raton, pp 177–233

Crumbliss AL, Harrington JM (2009) Iron sequestration by small molecules: thermodynamic and kinetic studies of natural siderophores and synthetic model compounds. In: van Eldik R, Hubbard CD (eds) Advances in inorganic chemistry, vol 61. Elsevier, New York, pp 179–250

Edwards JR, Turner PJ, Wannop C, Withnell ES, Grindey AJ, Nairn K (1989) In vitro antibacterial activity of SM-7338, a carbapenem antibiotic with stability to dehydropeptidase I. Antimicrob Agents Chemother 33:215–222

El-Maali NA (1998) Electrochemical behavior of the monobactam antibiotic aztreonam at different electrodes and in biological fluids. Bioelectrochem Bioenerg 45:281–286

Fenton HJH (1894) Oxidation of tartaric acid in presence of iron. J Chem Soc Trans 65:899–910

Forlani L, Tocke AL, Vecchio ED, Lakhdar S, Goumont R, Terrier F (2006) Assessing the nitrogen and carbon nucleophilicities of 2-aminothiazoles through coupling with superelectrophilic 4,6-dinitrobenzofuroxan. J Org Chem 71:5527–5537

Gans P, O'Sullivan B (2000) GLEE, a new computer program for glass electrode calibration. Talanta 51:33–37

Gans P, Sabatini A, Vacca A (1996) Investigation of equilibria in solution. Determination of equilibrium constants with HYPERQUAD suite of programs. Talanta 43:1739–1753

Harrington JM, Crumbliss AL (2009) The redox hypothesis in siderophore-mediated iron uptake. Biometals 22:679–689

Harris WR, Carrano CJ, Raymond KN (1979) Coordination chemistry of microbial iron transport compounds. 16. Isolation, characterization, and formation constants of ferric aerobactin. J Am Chem Soc 101:2722–2727

Martell AE, Motekaitis RJ (1992) Determination and use of stability constants. VCH Publ, New York

Miller MJ, Zhu H, Xu Y, Wu C, Walz AJ, Vergne A, Roosenberg JM, Moraski G, Minnick AA, McKee-Dolence J (2009) Utilization of microbial iron assimilation processes for the development of new antibiotics and inspiration for the design of new anticancer agents. Biometals 22:61–75

Pierre J-L, Fontecave M (1999) Iron and activated oxygen species in biology: the basic chemistry. Biometals 12:195–199

Pierre J-L, Fontecave M, Crichton RR (2002) Chemistry for an essential biological process: the reduction of ferric iron. Biometals 15:341–346

Ramunas J, Motekaitis RJ, Martell AE (1991) Stabilities of the iron(III) chelates of 1,2-dimethyl-3-hydroxy-4-pyridinone and related ligands. Inorg Chim Acta 183:71–80

Raymond KN, Dertz EA (2004) Biochemical and physical properties of siderophores. In: Crosa JH, Rey AR, Payne SM (eds) Iron transport in bacteria. ASM Press, Washington, DC, pp 5–17

Rolston KVI, Bodey GP (1992) *Pseudomonas aeruginosa* infection in cancer patients. Cancer Invest 10:43–59

Scarrow RC, Riley PE, Abu-Dari K, White DL, Raymond KN (1985) Ferric ion sequestering agents. 13. Synthesis, structures, and thermodynamics of complexation of cobalt(III) and iron(III) tris complexes of several chelating hydroxypyridinones. Inorg Chem 24:954–967

Sentochnik DE, Eliopoulos GM, Ferraro MJ, Moellering RC (1989) Comparative in vitro activity of SM7338, a new carbapenem antimicrobial agent. Antimicrob Agents Chemother 33:1232–1236

Stintzi A, Raymond KN (2002) Siderophore chemistry. In: Templeton DM (ed) Molecular and cellular iron transport. Marcel Dekker, Inc., New York, pp 273–320

Sykes RB (1988) The new monobactams: chemistry and biology. J Clin Pharmacol 28:113–119

Tipper DJ (1985) Mode of action of beta-lactam antibiotics. Pharmac Ther 27:1–35

Vogel AI (1961) A text-book of quantitative inorganic analysis. Longmans, Green, and Co Ltd, London

Williamson DS, Nagel DL, Markin RS, Cohen SM (1987) Effect of pH and ions in the electronic structure of saccharin. Food Chem Toxic 25:211–218

Zurenko GE, Truesdell SE, Yagi BH, Mourey RJ, Laborde AL (1990) In vitro antibacterial activity and interactions with beta-lactamases and penicillin-binding proteins of the new monocarbam antibiotic U-78608. Antimicrob Agents Chemother 34:884–888